A Matched CBCT Projector-Backprojector Based on the Convolution of B-splines

Marion Savanier, Cyril Riddell, Yves Trousset, Emilie Chouzenoux, Jean-Christophe Pesquet

A Matched CBCT Projector-Backprojector Based on the Convolution of B-splines

Marion Savanier[1,2], Cyril Riddell[1], Yves Trousset[1], Emilie Chouzenoux[2] and Jean-Christophe Pesquet[2]

***Abstract*—Discretizing tomographic operators is a crucial step in the design of reconstruction algorithms. In particular, for iterative methods, the projector and backprojector are usually assumed to be matched to guarantee convergence. In practice, the reconstruction task is challenging, especially in cone-beam geometry. To this end, in the context of CBCT with a flat panel detector, we propose to rely on an interpolating kernel based on the convolution of B-splines taking into account the sampling of the detector and of the volume. Matched CBCT projector/backprojector based on resampling transforms are designed.**

***Index Terms*—CBCT, discretization, matched pair, projector, backprojector, B-spline, flat-panel.**

I. Introduction

FLAT-panel based C-arm systems are widely used imaging tools for image-guidance in interventional radiology and surgery. In addition, cone-beam computed tomography (CBCT) allows planning, guidance and control of the procedure. C-arm CBCT often suffers from poor sampling rate. The potential of reconstructing undersampled data with non linear iterative algorithms has been demonstrated, for instance to reduce angular and cone-beam undersampling artifacts [1]. One may intentionally decrease the sampling to reduce the X-ray dose. In this context, we are particularly interested in least-squares based optimization criteria regularized with nonlinear terms [2]. Most penalized least-squares algorithms require the use of the forward operator (i.e., projector), and the associated backward operator (i.e., backprojector). The projector must encode the C-arm projective geometry as accurately as possible. Furthermore, an underlying symmetry assumption is made, as the backprojector is assumed to coincide with the algebraic adjoint of the projector. Most forward models assume a geometric voxel shape (e.g. cubic) and its projection onto the detector. When ray-tracing is chosen, the backprojection implementation is not efficient, so that alternative models have been proposed, namely the distance-driven [3] and the separable-footprint [4]. These implementations are generic enough to be used with CT scanners curved detector and C-arm flat panel. In the context of flat panel CBCT, the geometry can be described with projection matrices. These matrices continuously relate any point in space to any point over the detection surface. This naturally leads to modeling the volume as samples in space and the measurements as samples over the detector. Voxels are considered through their centers and no shape is assumed. Very efficient backprojection schemes, using resampling transforms, are derived and used for standard analytical reconstruction, where backprojection is required only. Unfortunately, they cannot be represented as being the adjoint of any of the aforementioned forward models, and thus do not secure the convergence of standard iterative minimization schemes. It is worth pointing out that, in practice, the combination of resampling transforms for backprojection and ray-tracing for forward projection has been used [5], with apparently limited consequences despite the violation of the symmetry condition. The main reason may be that most iterative schemes are run for few iterations only, so that convergence issues may not be detected. Resampling transforms have also been used for the forward projection and here again, symmetry remains an issue [6].

Optimal resizing based on the convolution of B-splines has been extensively studied by Unser et al. [7]. In this paper, we propose to extend this approach to the discretization of resampling homographies, the transforms involved in CBCT with flat panel. We thus derive novel matched pairs of projector/backprojector that allow for precise and efficient forward and backward modeling while keeping symmetry.

In Section II, we recall the decomposition of cone-beam projection/backprojection with projection matrices as a series of homographies and introduce the proposed convolution scheme. Numerical experiments are then provided and discussed in Section III to evaluate the image quality associated with these novel tomographic operators.

II. Proposed method

A. Projector and backprojector pair

Let $\mathbf{f} = (f_l)_{1\leq l\leq L} \in \mathbb{R}^L$ denote the unknown volume attenuation with L voxels, $\mathbf{p} = (p_k)_{1\leq k\leq K} \in \mathbb{R}^K$, the log-transformed of the K detector cell measurements acquired on a C-arm system, and $\mathbf{R} \in \mathbb{R}^{K\times L}$ the forward projection model, whose entries $(R_{k,l})_{1\leq k\leq K, 1\leq l\leq L}$ relate each detector cell k to each voxel l. Reconstruction aims to estimate volume $\mathbf{f}$ from the knowledge of $\mathbf{p}$ and $\mathbf{R}$, based on the linear observation model:

$$\mathbf{p} = \mathbf{R}\mathbf{f} + \mathbf{n}, \tag{1}$$

where $\mathbf{n}$ is an additive noise. Iterative penalized least-squares algorithms minimize the sum of a data fidelity term $\frac{1}{2}\|\mathbf{R}\mathbf{f} - \mathbf{p}\|_2^2$ and a regularizer embedding prior information, such as image smoothness or range constraints. They usually account for the least-squares term through its gradient of the form $\mathbf{B}(\mathbf{R}\mathbf{f} - \mathbf{p})$, where $\mathbf{B} \in \mathbb{R}^{L\times K}$ denotes the backprojection operator. Ideally, we should have $\mathbf{B} = \mathbf{R}^\top$. However, as

(1): GE Healthcare, Buc, France. E-mail: first.last@ge.com
(2): Univ. Paris-Saclay, CentraleSupélec, CVN, Inria, Gif-sur-Yvette, France. E-mail: first.last@centralesupelec.fr
This work was supported by the ANRT CIFRE Convention 2018/1587.

we will discuss hereafter, it may happen that the latter equality does not hold, possibly leading to convergence instabilities and image quality deterioration.

B. Cone-beam geometry

The projection geometry is defined by the relationship between voxel coordinates (x, y, z) and the coordinates of the projected pixels (u, v). In CBCT with a flat-panel detector, the projector is characterized by a set of 3×4 projection matrices. There is one projection matrix per position of the imaging system. For a given projection matrix $\boldsymbol{P}$, the coordinates (u, v) of the projection of (x, y, z) onto the detection plane Π can be written with homogeneous coordinates (su, sv, s), with $s \in \mathbb{R}$, as $\left(su, sv, s\right)^\top = \boldsymbol{P}\left(x, y, z, 1\right)^\top$. The projection operation being separable, its discretization can be decomposed into 1D homographies that relate one free variable in space, e.g. x, to another one over the detector, e.g. u. For instance,

$$\left(su, sv_0, s\right)^\top = \boldsymbol{P}\left(x, y_0, z_0, 1\right)^\top \tag{2}$$

reduces to

$$\left(su, s\right)^\top = \boldsymbol{H}\left(x, 1\right)^\top \tag{3}$$

with $\boldsymbol{H} = (h_{s,t})_{1 \le s,t \le 2}$ a 2×2 homographic matrix. This operation can be analytically recast as the 1D homographic function h:

$$u = h(x) = \frac{h_{1,1}x + h_{1,2}}{h_{2,1}x + h_{2,2}}. \tag{4}$$

Without loss of generality, we shall thus treat the projected data p and original data f as continuous 1D signals. Backprojection resamples f from p and reprojection resamples p from f according to $p(u) = p \circ h(x) = f \circ h^{-1}(u) = f(x)$.

Homography h captures the continuously varying sampling scale by the magnification factor given by derivative $h'(x)$. In our clinical context, the geometry has a large focal distance with respect to the field of view so that h is never singular and the magnification factor varies slowly around $h'(0) = \det \boldsymbol{H}/h_{2,2}^2$. Consequently, the inverse homography h^{-1} behaves in a similar way. The discretization defines index i spanning the subset of detector cell locations $(u_i)_{1 \le i \le I}$ and index j spanning the subset of voxel locations $(x_j)_{1 \le j \le J}$ that are seen through h, giving rise to the discrete signals $\mathbf{p} = (p(u_i))_{1 \le i \le I}$ and $\mathbf{f} = (f(x_j))_{1 \le j \le J}$.

To interpolate, one decomposes signals p and f onto a set of continuous basis functions. A famous family of basis functions is that of B-splines of order $n \in \mathbb{N}$ denoted by $\beta^n : \mathbb{R} \to \mathbb{R}$. The associated centered B-spline of order n and scale $\delta > 0$ is defined by $\beta^n_\delta = \beta^n(\cdot/\delta)$. The simplest B-spline, of order 0, leads to nearest neighbor interpolation, while order 1 corresponds to linear interpolation. For a given h, one defines $\delta_1 = 1$ and $\delta_2 = \delta_1 h'(0)$ as the sampling steps for f and p, respectively.

Backprojection operator $\mathbf{B}$ computes the values $(f_j)_{1 \le j \le J}$ from $(p_i)_{1 \le i \le I}$ of $\mathbf{p}$ using $p(u) = \sum_{i=1}^I p_i \beta^n_{\delta_2}(u - u_i)$ so that $B_{j,i} = \beta^n_{\delta_2}(h(x_j) - u_i)$. Conversely, projection operator $\mathbf{R}$ uses $f(x) = \sum_{j=1}^J f_j \beta^n_{\delta_1}(x - x_j)$ from the components $(f_j)_{1 \le j \in J}$ of $\mathbf{f}$ so that $R_{i,j} = \beta^n_{\delta_1}(h^{-1}(u_i) - x_j)$. To get a matched pair, one would replace $\mathbf{B}$ with $\mathbf{R}^\top$ which gives $f(x_j) = \sum_{i|j \in \Omega_i} p_i \beta^n_{\delta_1}(h^{-1}(u_i) - x_j)$ with Ω_i the set of indices j such that for a given i, $R_{i,j} \neq 0$. This expansion appears as a poor choice for computing f_j in a direct manner because it uses the basis functions $\beta^n_{\delta_1}$ instead of $\beta^n_{\delta_2}$. As a result, detector cells contribute with gaps or redundancies to image pixels, which leads to high frequency artifacts.

C. Convolution-based basis function

We now assume that p and f are decomposed onto sets of B-splines of possibly different orders, $n \in \mathbb{N}$ for p and $m \in \mathbb{N}$ for f.

To overcome the previously described limitation, we propose to use a basis function suitable for both projection and backprojection, the latter requiring to capture $\beta^n_{\delta_1} \circ h^{-1}(u)$. For this purpose, we define the interpolating kernel $\phi^{m,n}_{\delta_1,\Delta_{1,i}}$ made of the normalized convolution of basis functions $\beta^m_{\delta_1}$ and $\beta^n_{\Delta_{1,i}}$ with $\Delta_{1,i} = (h^{-1})'(u_i)\delta_1$. Without loss of generality, we set $\delta_1 = 1$, and $\Delta_{1,i}$ is interpreted as a sampling parameter for the variation of magnification induced by the homography. The projection sampled at locations $(u_i)_{1 \le i \le I}$ now reads:

$$\begin{aligned} p_i = f(h^{-1}(u_i)) = (\mathbf{R}\mathbf{f})_i &= \sum_{j=1}^J f_j \phi^{m,n}_{1,\Delta_{1,i}}(h^{-1}(u_i) - x_j) \\ &= \sum_{j=1}^J \frac{f_j}{\Delta_{1,i}} \left(\beta^n_{\Delta_{1,i}} * \beta^m_1\right)(h^{-1}(u_i) - x_j) \end{aligned} \tag{5}$$

with $R_{i,j} = \frac{1}{\Delta_{1,i}} \left(\beta^n_{\Delta_{1,i}} * \beta^m_1\right)(h^{-1}(u_i) - x_j)$. From the general scaling property, for every $\Delta > 0$, $\left(\beta^n_\Delta * \beta^m_1\right)(u) \equiv \Delta \left(\beta^n_1 * \beta^m_{\frac{1}{\Delta}}\right)(u/\Delta)$. This allows us to deduce the adjoint of matrix $\mathbf{R}$ aiming at computing the backprojection at locations $(x_j)_{1 \le j \le J}$:

$$\begin{aligned} f_j = (\mathbf{R}^\top \mathbf{p})_j &= \sum_{i=1}^I \frac{p_i}{\Delta_{1,i}} \left(\beta^n_{\Delta_{1,i}} * \beta^m_1\right)\left(h^{-1}(u_i) - x_j\right) \\ &= \sum_{i=1}^I p_i \left(\beta^n_1 * \beta^m_{\frac{1}{\Delta_{1,i}}}\right)\left(\frac{h^{-1}(u_i) - x_j}{\Delta_{1,i}}\right) \\ &= \sum_{i=1}^I p_i \left(\beta^n_1 * \beta^m_{\frac{1}{\Delta_{1,i}}}\right)\left(u_i - \frac{x_j}{\Delta_{1,i}}\right). \end{aligned} \tag{6}$$

Similarly, we can express $\mathbf{B}$ using the normalized convolution $\frac{1}{\Delta_{2,j}} \left(\beta^m_{\Delta_{2,j}} * \beta^n_1\right)$. The backprojected function at locations $(u_j)_{1 \le j \le J}$ can then be computed as

$$\begin{aligned} f_j = p(h(x_j)) &= \sum_{i=1}^I \frac{p_i}{\Delta_{2,j}} \left(\beta^n_1 * \beta^m_{\Delta_{2,j}}\right)(h(x_j) - u_i) \\ &= \sum_{i=1}^I \frac{p_i}{\Delta_{2,j}} \left(\beta^n_1 * \beta^m_{\Delta_{2,j}}\right)(\Delta_{2,j}x_j - u_i). \end{aligned} \tag{7}$$

The coefficients of matrix $\mathbf{B}$ are thus $B_{j,i} = \frac{1}{\Delta_{2,j}} \left(\beta^n_1 * \beta^m_{\Delta_{2,j}}\right)(h(x_j) - u_i)$. From (7) and (6), we still have $\mathbf{B}^\top \neq \mathbf{R}$, but, up to a normalization factor, the difference now comes from our linear approximation to the homography h, quantified by the set of magnification

factors $(\Delta_{2,j})_{1\leq j\leq J}$ and $(1/\Delta_{1,i})_{1\leq i\leq I}$. The precision of our model relies on two factors, namely the order of the B-spline[1], and the set of magnifications. The former point is well documented and one can easily select the best trade-off between precision and complexity for a given application. Regarding magnification factors, neither the projector nor the backprojector is worthy to be privileged. In (6), $\Delta_{1,i}$ could be replaced by $\Delta_{2,j}$. The largest set of magnifications should be chosen to better capture the changes in sampling rates induced by h and h^{-1}.

D. Implementation

Since detectors are composed of cells, we choose to represent p with zero order B-spline, β_1^0 i.e. $n = 0$. We do not restrict the volume to be a set of cubic voxels and we keep the flexibility $m \in \{0, 1\}$ for f. Let us set $\Delta > 0$. The scaled convolution kernel $\phi_{1,\Delta}^{m,0}$ is such that

$$\phi_{1,\Delta}^{m,0}(\ell) = \frac{1}{\Delta}(\beta_1^m * \beta_\Delta^0)(\ell) = \frac{1}{\Delta}\int_{-\infty}^{+\infty} \beta_1^m(\tau)\beta_\Delta^0(\ell-\tau)d\tau, \tag{8}$$

for $\ell \in \mathbb{R}$. The latter kernel gives the interpolation values at $(x_j)_{1\leq j\leq J}$ and $(u_i)_{1\leq i\leq I}$. In addition, if B-splines of order 1 are chosen for function f (i.e. $m = 1$), once the entries of $\mathbf{f} = (f(x_j))_{1\leq j\leq J}$ have been computed with $\mathbf{B}$, a digital post-filter to $\mathbf{f}$ corresponding to the cubic spline interpolation filter must be applied to $\mathbf{f}$ as demonstrated in [7].

Given our choices for n and m, we are interested in two interpolating kernels: $\phi_{1,\Delta}^{0,0}$ and $\phi_{1,\Delta}^{1,0}$. Before deriving their explicit formula from (8), let us recall the formula of the B-splines of order 0 and 1, for every $\ell \in \mathbb{R}$:

$$\beta^0(\ell) = \begin{cases} 1 & \text{if } |\ell| < \frac{1}{2} \\ 0 & \text{otherwise,} \end{cases}$$

$$\beta^1(\ell) = \begin{cases} 1-|\ell| & \text{if } |\ell| < 1 \\ 0 & \text{otherwise.} \end{cases}$$

- **Case 1**

$$\phi_{1,\Delta}^{0,0}(\ell) = \begin{cases} \min(1,\Delta)/\Delta & \text{if} \quad |\ell| < a_1 \\ \frac{1}{\Delta}(a_2 - |\ell|) & \text{if} \quad a_1 \leq |\ell| < a_2 \\ 0 & \text{if} \quad |\ell| \geq a_2 \end{cases}$$

  with $a_1 = \frac{|\Delta-1|}{2}$, and $a_2 = \frac{\Delta+1}{2}$.

- **Case 2**

$$\phi_{1,\Delta}^{1,0}(\ell) = \begin{cases} c_{k,0} + c_{k,1}|\ell| + c_{k,2}\ell^2 & \text{for } |\ell| \in [a_{k-1}, a_k) \\ & \text{and } k \in \{1,2\} \\ 0 & \text{otherwise} \end{cases}$$

  with $a_0 = 0$, $a_1 = |\frac{\Delta}{2} - 1|$, $a_2 = \frac{\Delta}{2} + 1$ and expressions for $(c_{k,0}, c_{k,1}, c_{k,2})$ are given in Tab. I.

The approach of lowest order is comparable in complexity to linear interpolation and is thus simpler than original distance-driven. Kernels of higher degree increase computation time proportionally to their larger support.

[1]None of the above calculations rely on the fact that the basis functions are B-splines. Thus, one could easily choose another class of functions, noting that B-splines functions enjoy the minimal support for a given approximation order and the maximal approximation order for a given support.

Interval	$c_{k,0}$	$c_{k,1}$	$c_{k,2}$
$\lvert\ell\rvert < a_1$			
if $\Delta \leq 2 \wedge \lvert\ell\rvert < \Delta/2$	$1 - \Delta/4$	0	$-\frac{1}{\Delta}$
if $\Delta \leq 2 \wedge \lvert\ell\rvert \geq \Delta/2$	1	-1	0
if $\Delta > 2$	$1/\Delta$	0	0
$a_1 \leq \lvert\ell\rvert < a_2$			
if $\lvert\ell\rvert \geq \Delta/2$	$(\Delta + 4 + 4/\Delta)/8$	$-\frac{1}{\Delta} + \frac{1}{2}$	$-\frac{1}{2\Delta}$
if $\lvert\ell\rvert < \Delta/2$	$(-\Delta + 4 + 4/\Delta)/8$	$-\frac{1}{\Delta} - \frac{1}{2}$	$\frac{1}{2\Delta}$

TABLE I: B-spline parameters for case 2

III. Experiments

A. Simulation context

To prove the concept of our approach, we evaluated our projector and backprojector as single modules and within an iterative reconstruction task. We computed simulated noise-free data of geometrical phantoms in CBCT geometry of half cone angle of 20°, as can be found on clinical C-arm systems. The detector bins are sampled on a finer grid than the voxels leading to a magnification of factor $\sqrt{2}$. Linear interpolation was taken as a baseline, for projector/backprojector construction and the distance-driven pair (DD) was added to the comparison. First, we analyzed the performance of matrix $\mathbf{R}$ for the B-splines kernels when projecting a centered uniform cylinder of attenuation 0.1 per voxels of diameter 80 voxels over $360°$. The scanned object being invariant by rotation, we quantified the rotation invariance by computing the root mean-square error (RMSE) and the maximum error (MAE) between each profile over the range $[0°, 45°]$ and profile at angle $0°$. Then, for the same task, we compared the performance of the transpose of matrix $\mathbf{B}$. Finally we evaluated the spatial resolution associated to the different interpolation kernels using the modulation transfer function (MTF) on the reconstruction of a cube from 600 projections over $360°$. To avoid the inverse crime, the forward-projection data was calculated with a 3000×20 pixel detector that was rebinned to 750×20 pixels. An FDK reconstruction was first performed to investigate the quality of $\mathbf{R}^\top$ and $\mathbf{B}$ as backprojectors. Then an iterative reconstruction was performed by applying 500 Landweber iterations with $\mathbf{f}^{(0)}$ chosen as the zero vector:

$$\mathbf{f}^{(n+1)} = \mathbf{f}^{(n)} - \tau\mathbf{R}^\top(\mathbf{R}\mathbf{f}^{(n)} - \mathbf{p}), \quad n \in \mathbb{N}. \tag{9}$$

Parameter τ is chosen as $1.9/\|\mathbf{R}\|^2$. No regularization was added as we aim to highlight features that are intrinsic to the model. This experiment gives an insight on the largest singular values of operator $\mathbf{R}$. Since the reconstruction methods investigated here are linear, spatial resolution at a slanted edge (tilting of $5°$) is a suitable MTF.

B. Results

For the projection of the uniform cylinder, with $\mathbf{R}$, upon visual inspection of plotted profiles, the results are very similar for all interpolation schemes (plots not shown). For both invariance metrics, the convolution kernel $\phi^{1,0}_{\cdot}$ combined with

a digital filter provides slightly better results: RMSE is 0.008 and MAE is 0.044 at angle $0°$ and monotonically increases up to 0.178 and 1.052 at $45°$ while the other schemes perform almost identically (RMSE of 0.04 and MAE of 0.213 at $0°$, RMSE of 0.185 and MAE of 1.09 at $45°$). With $\mathbf{B}^\top$, the profile of the projected cylinder at the angle $45°$ resulting from the transpose of linear interpolation is clearly distinguishable as it is degraded by high-frequency oscillations, which do not appear with any of the other convolutional basis functions (profiles not shown). The RMSE and MAE scores corroborate this observation.

Figure 1 displays the MTF curves obtained for the FDK reconstruction task with $\mathbf{B}$. For this task, $\phi_{\cdot}^{0,0}$ and DD scheme

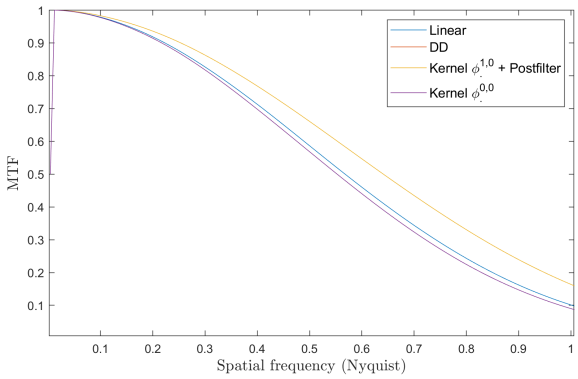

Fig. 1: MTF curve for $\mathbf{B}$

provides superimposed MTF curves just below the curve obtained with linear interpolation. Kernel $\phi_{\cdot}^{1,0}$ combined with a digital filter for the backprojection produces better spatial resolution. We further quantitatively compare their MTF curves through frequency $\nu_{0.2}$ for which the MTF reaches value 0.2. For kernel $\phi_{\cdot}^{1,0}$, $\nu_{0.2}$ is increased by 0.1. Then for FDK reconstruction with $\mathbf{R}^\top$, the same frequencies $\nu_{0.2}$ are tabulated in Table II. All MTF curves are close with a slight advantage for $\phi_{\cdot}^{0,0}$.

	Linear	DD	$\phi_{\cdot}^{0,0}$	$\phi_{\cdot}^{1,0}$
$\nu_{0.2}$	0.808	0.824	0.824	0.793

TABLE II: Spatial frequency $\nu_{0.2}$ at 20% MTF for FDK with $\mathbf{R}^\top$

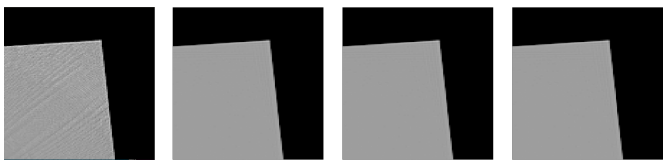

Fig. 2: Zoom on corner of reconstructed slice. From left to right: Linear interpolation, DD, $\phi_{\cdot}^{0,0}$, $\phi_{\cdot}^{1,0}$.

Finally, after 500 Landweber iterations, the reconstructed square with linear interpolation is substantially different than those obtained with the other models as shown on Figure 2. Undesirable interpolation patterns are visible with linear interpolation. This indicates that some non-null singular values of such $\mathbf{R}$ are of very low magnitude, yielding a reconstruction with details similar to discretization errors. For the other models, frequencies $\nu_{0.2}$ are reported in Table III. All MTF curves are almost superimposed: $\phi_{\cdot}^{0,0}$, $\phi_{\cdot}^{1,0}$ and DD scheme produce sharp reconstructions, comparable to that of FDK.

	DD	$\phi_{\cdot}^{0,0}$	$\phi_{\cdot}^{1,0}$
$\nu_{0.2}$	0.8945	0.8945	0.8711

TABLE III: Spatial frequency $\nu_{0.2}$ at 20% MTF for iterative reconstruction

These preliminary results suggest that the transpose of the linear interpolation-based backprojection does not qualify as a quality projection model. By using a refined discretization of the resampling transform through our convolution kernels, the performance of the transpose becomes similar to that of direct models for the basic tests given here, even with the lowest order of B-spline. Our results indicate that the kernel obtained with B-splines of order 0 perform as well as the distance-driven pair in a consistent fashion. This scheme is based on a similar rationale as ours, but is not flexible as it does not provide means for higher–order interpolation. We did not get consistent MTF increases when raising the degree of the spline modeling the volume. Further experiments are needed to tell whether it can improve reconstruction of real data at a reasonable computation cost. As advocated in [6], iterative reconstruction could have been performed in a virtual geometry, called rectified geometry. On the one hand, it incurs an additional resampling step that may degrade precision. On the other hand, homographies reduce to magnifications. The resampling task is simplified into that of the resizing problem for which the B-splines approach chosen here benefits from strong theoretical properties [7], especially in terms of optimal approximation.

IV. Conclusion

A novel interpolation scheme based on B-spline convolution has been proposed to discretize the projector and backprojector, in the context of CBCT with a flat panel detector. The expected benefits of this approach is improved reconstruction for various methods involving a matched pair of projector/backprojector requiring high-quality interpolation.

References

[1] H. Langet, C. Riddell, A. Reshef, Y. Trousset, A. Tenenhaus, E. Lahalle, G. Fleury, and N. Paragios, "Compressed-sensing-based content-driven hierarchical reconstruction: Theory and application to c-arm cone-beam tomography," *Medical Physics*, vol. 42, Aug. 2015.

[2] C. Chaux, P. L. Combettes, J.-C. Pesquet, and V. R. Wajs, "A variational formulation for frame based inverse problems," *Inverse Problems*, vol. 23, no. 1, Jun. 2007.

[3] B. De Man and S. Basu, "Distance-driven projection and backprojection in three dimensions," *Physics in medicine and biology*, vol. 49, July 2004.

[4] Y. Long, J. A. Fessler, and J. M. Balter, "3D forward and back-projection for x-ray ct using separable footprints," *IEEE Transactions on Medical Imaging*, vol. 29, no. 11, Nov. 2010.

[5] R. R. Galigekere, K. Wiesent, and D. W. Holdsworth, "Cone-beam reprojection using projection-matrices," *IEEE Transactions on Medical Imaging*, vol. 22, no. 10, Oct. 2003.

[6] C. Riddell and Y. Trousset, "Rectification for cone-beam projection and backprojection," *IEEE Transactions on Medical Imaging*, vol. 25, no. 7, July 2006.

[7] M. Unser, A. Aldroubi, and M. Eden, "Enlargement or reduction of digital images with minimum loss of information," *IEEE Transactions on Image Processing*, vol. 4, no. 3, March 1995.